Chiral twisted van der Waals nanowires

Peter Sutter,[1] Shawn Wimer,[1] and Eli Sutter[2,*]

[1]Department of Electrical & Computer Engineering; [2]Department of Mechanical & Materials Engineering, University of Nebraska-Lincoln, Lincoln, NE 68588, United States

Van der Waals heterostructures with small misalignment between adjacent layers ('interlayer twist') are of interest due to emerging electronic structure and correlation phenomena that are determined both by the atomic lattice and long-range superlattice potentials arising in interlayer moiré patterns.[1-7] To date, such twisted heterostructures have involved a single planar interface between layers isolated by exfoliation and micromechanically stacked in the desired relative orientation.[1,8-12] Here, we demonstrate a class of materials, van der Waals nanowires of layered crystals, in which tunable interlayer twist naturally evolves during the growth process. In a vapor-liquid-solid growth process, nanowires of germanium (II) sulfide (GeS), an anisotropic layered semiconductor, crystallize with layering along the wire axis[15] and have a strong propensity for forming axial screw dislocations. Nanometer-resolved electron diffraction shows that Eshelby twist, induced by a torque on the ends of a cylindrical solid due to the stress field of an axial dislocation,[16,17] causes a chiral structure of the van der Waals nanowires. The in-plane GeS crystal axes progressively rotate along the wire and GeS layers in adjacent turns of the helix naturally form a moiré pattern due to their interlayer twist. The axial rotation and the twist moiré are tunable via the nanowire thickness. Combined electron diffraction and cathodoluminescence spectroscopy show the correlation between the interlayer twist and locally excited light emission due to progressive changes in the lattice orientation and interlayer moiré registry along the nanowires. The findings demonstrate an approach toward the scalable fabrication of van der Waals structures with defined twist angles, for which interlayer moirés are realized along a helical path on a nanowire instead of a planar interface.

3D crystalline (Si, Ge, GaAs, etc.) semiconductor nanowires have long attracted interest as a class of nanomaterials that can be synthesized with exceptionally high crystal quality using vapor-liquid-solid (VLS) growth, in which a nanoscale liquid 'catalyst' transports source material from the vapor phase to the growth front of a solid, crystalline wire.[13,14] Previous work on integrating layered crystals in nanowires includes VLS growth of semiconducting SnS,[18] SnSe,[19] GaSe,[20] In_2Se_3[21] and Sb_2Se_3[22] wires, as well as Bi_2Te_3 and Bi_2Se_3 topological insulators[23]. Roughly half of these reports showed van der Waals stacking perpendicular and parallel to the nanowire axis, respectively. Here we focus on layered GeS nanowires synthesized by Au-catalyzed low-temperature VLS growth, which are particularly interesting due to their anisotropic structure. A robust synthesis (see Methods), discussed in detail elsewhere,[15] provides GeS nanowires with different diameters and uniform structure. The wires crystallize with van der Waals layering (*c*-axis) along their symmetry axis, i.e., the *a*- and *b* unit vectors spanning the individual anisotropic, covalently bonded layers lie in planes perpendicular to the wire (Fig. 1 a,

b). These structural characteristics are borne out in high-resolution images obtained by transmission electron microscopy (TEM) and high-angle annular dark-field scanning TEM (HAADF-STEM), which show lattice fringes with the GeS *c*-axis spacing of 1.06 nm across the nanowires, and by nanobeam electron diffraction (Fig. 1 c). Nanometer-scale diffraction, which can probe the local crystal orientation along the wires, shows another key property of the nanowire structure. Even if the crystal is locally aligned such that the electron beam projects along a low-index zone axis (here ZA ~ [1 0 0], Fig. 1 c) the diffraction patterns rotate systematically away from this orientation as the beam is displaced along the nanowire. While the GeS *c*-axis remains oriented along the wire, the (*a*, *b*) plane progressively rotates with a fixed helicity, i.e., the nanowires are chiral. For the wire shown in Fig. 1, for instance, the cumulative effect is to rotate the (*a*, *b*) plane by ~21° over a distance of 1.8 μm.

Imaging and further diffraction analysis of the GeS nanowire crystallography clarifies the origin of the observed unidirectional lattice rotation. In (S)TEM images, the registry of lattice fringes across the wires shows ubiquitous axial screw dislocations in the GeS van der Waals nanowires (Extended Data Fig. 1), consistent with the facile formation of screw dislocations or growth spirals in layered crystals,[24] including GeS,[25] SnS,[26], etc. Examination of the spatially resolved diffraction data for nanowires with different diameters identifies two key characteristics (Fig. 2 a): The cumulative lattice rotation increases linearly with displacement along the wires; and the rate of this increase shows a clear dependence on the nanowire diameter, with thinner wires rotating by larger angles per unit length. The mean rotation rate depends exponentially on the nanowire diameter across the size range accessed here (Fig. 2 b), reaching ~0.1° per nm for nanowires below 40 nm thickness. The presence of axial screw dislocations and the diameter dependent twist are telltale signatures of Eshelby twist, induced by a torque on the ends of a cylindrical solid due to the stress field of an axial dislocation, as the origin of the chiral structure of the van der Waals nanowires. The Eshelby formalism[16] relates the lattice rotation per unit length, $d\theta/dz$, to the cross-sectional area πR^2 of the cylinder and the Burgers vector $\boldsymbol{b}$ of the screw component of the axial dislocation: $d\theta/dz = \boldsymbol{b}/[\pi R^2]$. Replotting our data as a function of the nanowire footprint confirms the realization of Eshelby twist in the dislocated van der Waals nanowires, similar to previous results for conventional 3D crystalline nanowires,[17] and it allows extracting the Burgers vector of the axial screw dislocation (Fig. 2 c). From the diameter-dependent mean twist we find a mean magnitude of the Burgers vector $|\boldsymbol{b}| = (1.5 \pm 0.15)$ nm, corresponding to about 1.5 times the *c*-axis dimension of the GeS unit cell (Computed: 1.077 nm;[27] experimental: 1.042 nm),[28] which contains two weakly coupled GeS layers spaced by L = 0.521 nm. An alternative analysis using the full position dependent diffraction data set of Fig. 2 a confirms this mean value of $|\boldsymbol{b}|$ but provides more detailed insight into the distribution of Burgers vectors (Fig. 2 d). It shows a preference for Burgers vectors of 1 and 2 *c*-axis unit cells (2 or 4 GeS layer spacings, L, respectively; Fig. 2 d, inset) and a suppression of small half-integer values. The overall Gaussian line shape of the histogram is consistent with the expected progressive reduction of the frequency for larger Burgers vectors.

The crystallographic analysis shows that the layered GeS nanowires are helical growth spirals

with diameter dependent crystal twist that predominantly involves 1 or 2 GeS unit cells, i.e., 2 or 4 layers. The helicity implies the spontaneous formation of interlayer twist between the lattices in adjacent turns of the spiral, analogous to the twist achieved by artificial stacking of extended two-dimensional or layered crystals.[1,7] Similar to planar systems such as twisted bilayer graphene,[5,6] this interlayer twist between identical two-dimensional crystals generates a rotational moiré pattern that sets up a spatially varying superlattice potential at the twisted van der Waals interface (Fig. 2 e). Due to the large moiré period (Extended Data Fig. 2) and the way the twist moiré is projected onto a helical van der Waals interface along the nanowires (see Methods, Extended Data Fig. 10), the direct probing of the moiré pattern by diffraction is not feasible. To detect signatures of the crystal rotation and interlayer moiré via the expected changes in electronic structure, we carried out cathodoluminescence spectroscopy excited locally by the focused electron beam in STEM. Results of such STEM-CL measurements are shown in Fig. 3.

Combined nanobeam electron diffraction and STEM-CL measured at room temperature show the correlation between the progressive interlayer twist, here ~17° over 420 nm in length (Fig. 3 a), and locally excited light emission from the nanowires. Series of CL spectra obtained along individual GeS nanowires show that the cumulative twist along the wire is accompanied by synchronous changes in the intensity, width, and center wavelength of the GeS band edge luminescence (Fig. 3 c). Specifically, the center wavelength shifts from ~580 nm to a minimum of 530 nm while the peak width increases from ~170 nm to 260 nm. Over the same distance the amplitude of the Gaussian peak decreases by ~25%. Similar systematic changes in the spectral characteristics were obtained in STEM-CL at low temperature (T = 110 K; Extended Data Fig. 3). The center wavelength of the nanowire luminescence is strongly blue-shifted from the GeS bulk bandgap (1.60 eV)[29] and scales inversely with the wire diameter, suggesting a confinement effect (Extended Data Figs. 4, 5). However, since the Eshelby twist also increases with decreasing diameter (Fig. 2), an effect of the twist on the bandgap cannot be excluded. The large peak width is the result of inhomogeneous line broadening. In STEM-CL, an entire chain of elementary processes, excitation, transport by diffusion or drift, and ultimately recombination is involved prior to photon emission.[30] Control experiments show the redistribution of excited charge carriers due to electric-field induced drift, likely due to the filling of trap states at the core of the axial screw dislocation (see Methods). Hence, despite the local electron beam excitation a finite section of the nanowire – covering a range of electronic structure (e.g., bandgap) – is involved in light emission, which produces the observed broad luminescence peaks.

For chiral GeS nanowires the position-dependent changes in the luminescence spectra could originate from two distinct effects: The progressive rotation of the van der Waals layers (i.e., of the (*a*, *b*) crystal axes) with respect to the exciting electron beam, or gradual changes in electronic structure due to a varying interlayer moiré registry. The electron beam excitation and light collection in STEM-CL are largely isotropic and should not be sensitive to rotation of the anisotropic GeS lattice,[29] but bandstructure effects on the light emission for different incidence directions of the exciting electron beam cannot be ruled out entirely. Raman scattering and

photoluminescence (PL) spectroscopy of GeS plates excited by linearly polarized light incident along the *c*-axis show a strong polarization dependence of the Raman intensity of the major (B_{3g}, A_g) phonon modes, but only a small modulation of the PL intensity and no significant shifts of the emission wavelength (Extended Data Fig. 6). Hence, the systematic changes in luminescence shown in Fig. 3 likely arise from modifications to the electronic structure due to a progressively varying interlayer moiré registry along the nanowires. An analysis of STEM-CL spectra obtained along extended (several μm) sections of GeS van der Waals nanowires shows spectral features correlated with the local moiré registry, and thus supports the notion that changes in the twist moiré registry along the helical wires produce systematic variations in the electronic structure and optoelectronic properties (Supporting Note 2).

Layered nanowires can therefore be expected to harbor emergent electronic phenomena found so far only in planar van der Waals heterostructures. Layered semiconductors, as shown here, promise modulated optoelectronic properties due the twist superlattice[4] and chiral light-matter interactions[31] governed by both the helical structure and twist moiré. Realizing chiral wires from graphitic carbon would create a new platform for studying electron correlation effects of twisted bilayer graphene.[5,6] The one-dimensional geometry has several attributes distinct from conventional two-dimensional van der Waals stacks: Chiral nanowires spontaneously generate an interlayer moiré via Eshelby twist associated with axial screw dislocations; the twist angle and moiré periodicity are tunable via the nanowire diameter, which in turn can be selected by adjusting the size of the VLS catalyst;[32] and the moiré registry varies systematically along a helical path instead of an extended planar interface. Since layered crystals readily form screw dislocations, chiral nanowires may be produced from different materials covering a wide range of electronic structure, provided that they crystallize with van der Waals stacking parallel to the wire axis. In addition to progressively changing optoelectronic properties detected here by locally excited optical spectroscopy, measurements of gated transport along the GeS wires (Extended Data Fig. 7) demonstrate that van der Waals nanowires readily support measurements of charge transport along helical twist moirés. Hence, chiral nanowires represent a versatile platform for exploring phenomena associated with variable interlayer twist in layered materials.

References

1. Dean, C. R., Wang, L., Maher, P., Forsythe, C., Ghahari, F., Gao, Y., Katoch, J., Ishigami, M., Moon, P., Koshino, M., Taniguchi, T., Watanabe, K., Shepard, K. L., Hone, J. & Kim, P. Hofstadter's butterfly and the fractal quantum Hall effect in moiré superlattices. *Nature* **497**, 598 (2013).
2. Liu, K., Zhang, L., Cao, T., Jin, C., Qiu, D., Zhou, Q., Zettl, A., Yang, P., Louie, S. G. & Wang, F. Evolution of interlayer coupling in twisted molybdenum disulfide bilayers. *Nature Communications* **5**, 4966 (2014).
3. Yeh, P.-C., Jin, W., Zaki, N., Kunstmann, J., Chenet, D., Arefe, G., Sadowski, J. T., Dadap, J. I., Sutter, P., Hone, J. & Osgood, R. M. Direct Measurement of the Tunable Electronic Structure of Bilayer MoS2 by Interlayer Twist. *Nano Letters* **16**, 953-959 (2016).
4. Carr, S., Massatt, D., Fang, S., Cazeaux, P., Luskin, M. & Kaxiras, E. Twistronics: Manipulating the electronic properties of two-dimensional layered structures through their twist angle. *Physical Review B* **95**, 075420 (2017).

5. Cao, Y., Fatemi, V., Fang, S., Watanabe, K., Taniguchi, T., Kaxiras, E. & Jarillo-Herrero, P. Unconventional superconductivity in magic-angle graphene superlattices. *Nature* **556**, 43 (2018).
6. Cao, Y., Fatemi, V., Demir, A., Fang, S., Tomarken, S. L., Luo, J. Y., Sanchez-Yamagishi, J. D., Watanabe, K., Taniguchi, T., Kaxiras, E., Ashoori, R. C. & Jarillo-Herrero, P. Correlated insulator behaviour at half-filling in magic-angle graphene superlattices. *Nature* **556**, 80 (2018).
7. Ribeiro-Palau, R., Zhang, C., Watanabe, K., Taniguchi, T., Hone, J. & Dean, C. R. Twistable electronics with dynamically rotatable heterostructures. *Science* **361**, 690-693 (2018).
8. Yankowitz, M., Xue, J., Cormode, D., Sanchez-Yamagishi, J. D., Watanabe, K., Taniguchi, T., Jarillo-Herrero, P., Jacquod, P. & LeRoy, B. J. Emergence of superlattice Dirac points in graphene on hexagonal boron nitride. *Nature Physics* **8**, 382 (2012).
9. Ponomarenko, L. A., Gorbachev, R. V., Yu, G. L., Elias, D. C., Jalil, R., Patel, A. A., Mishchenko, A., Mayorov, A. S., Woods, C. R., Wallbank, J. R., Mucha-Kruczynski, M., Piot, B. A., Potemski, M., Grigorieva, I. V., Novoselov, K. S., Guinea, F., Fal'ko, V. I. & Geim, A. K. Cloning of Dirac fermions in graphene superlattices. *Nature* **497**, 594 (2013).
10. Kim, K., Yankowitz, M., Fallahazad, B., Kang, S., Movva, H. C. P., Huang, S., Larentis, S., Corbet, C. M., Taniguchi, T., Watanabe, K., Banerjee, S. K., LeRoy, B. J. & Tutuc, E. van der Waals Heterostructures with High Accuracy Rotational Alignment. *Nano Letters* **16**, 1989-1995 (2016).
11. Kang, K., Lee, K.-H., Han, Y., Gao, H., Xie, S., Muller, D. A. & Park, J. Layer-by-layer assembly of two-dimensional materials into wafer-scale heterostructures. *Nature* **550**, 229 (2017).
12. Frisenda, R., Navarro-Moratalla, E., Gant, P., Pérez De Lara, D., Jarillo-Herrero, P., Gorbachev, R. V. & Castellanos-Gomez, A. Recent progress in the assembly of nanodevices and van der Waals heterostructures by deterministic placement of 2D materials. *Chemical Society Reviews* **47**, 53-68 (2018).
13. Wagner, R. S. & Ellis, W. C. Vapor-Liquid-Solid Mechanism of Single Crystal Growth. *Applied Physics Letters* **4**, 89-90 (1964).
14. Morales, A. M. & Lieber, C. M. A laser ablation method for the synthesis of crystalline semiconductor nanowires. *Science* **279**, 208-211 (1998).
15. Sutter, E. & Sutter, P. 1D Wires of 2D Layered Materials: Germanium Sulfide Nanowires as Efficient Light Emitters. *ACS Applied Nano Materials* **1**, 1042-1049 (2018).
16. Eshelby, J. D. Screw Dislocations in Thin Rods. *Journal of Applied Physics* **24**, 176-179 (1953).
17. Bierman, M. J., Lau, Y. K. A., Kvit, A. V., Schmitt, A. L. & Jin, S. Dislocation-Driven Nanowire Growth and Eshelby Twist. *Science* **320**, 1060-1063 (2008).
18. Suryawanshi, S. R., Warule, S. S., Patil, S. S., Patil, K. R. & More, M. A. Vapor–Liquid–Solid Growth of One-Dimensional Tin Sulfide (SnS) Nanostructures with Promising Field Emission Behavior. *ACS Applied Materials & Interfaces* **6**, 2018-2025 (2014).
19. Liu, S., Guo, X., Li, M., Zhang, W.-H., Liu, X. & Li, C. Solution-Phase Synthesis and Characterization of Single-Crystalline SnSe Nanowires. *Angewandte Chemie International Edition* **50**, 12050-12053 (2011).
20. Peng, H., Meister, S., Chan, C. K., Zhang, X. F. & Cui, Y. Morphology Control of Layer-Structured Gallium Selenide Nanowires. *Nano Letters* **7**, 199-203 (2007).
21. Zhai, T., Fang, X., Liao, M., Xu, X., Li, L., Liu, B., Koide, Y., Ma, Y., Yao, J., Bando, Y. & Golberg, D. Fabrication of High-Quality In2Se3 Nanowire Arrays toward High-Performance Visible-Light Photodetectors. *ACS Nano* **4**, 1596-1602 (2010).
22. Yang, R. B., Bachmann, J., Pippel, E., Berger, A., Woltersdorf, J., Gösele, U. & Nielsch, K. Pulsed Vapor-Liquid-Solid Growth of Antimony Selenide and Antimony Sulfide Nanowires. *Advanced Materials* **21**, 3170-3174 (2009).
23. Alegria, L. D., Yao, N. & Petta, J. R. MOCVD synthesis of compositionally tuned topological insulator nanowires. *physica status solidi (RRL) – Rapid Research Letters* **8**, 991-996 (2014).

24. Burton, W. K., Cabrera, N. & Frank, F. C. The growth of crystals and the equilibrium structure of their surfaces. *Philosophical Transactions of the Royal Society of London. Series A, Mathematical and Physical Sciences* **243**, 299-358 (1951).
25. Bletskan, D. Production of GeS Single Crystals, Investigation of their Morphology and of Latter Influence on Hologram Recording. *Kristallografiya+* **20**, 1008-1012 (1975).
26. Sutter, P. & Sutter, E. Growth Mechanisms of Anisotropic Layered Group IV Chalcogenides on van der Waals Substrates for Energy Conversion Applications. *ACS Applied Nano Materials* **1**, 3026-3034 (2018).
27. Jain, A., Ong, S. P., Hautier, G., Chen, W., Richards, W. D., Dacek, S., Cholia, S., Gunter, D., Skinner, D., Ceder, G. & Persson, K. A. Commentary: The Materials Project: A materials genome approach to accelerating materials innovation. *APL Materials* **1**, 011002 (2013).
28. Bissert, G. & Hesse, K. F. Verfeinerung der Struktur von Germanium (II)-Sulfid, GeS. *Acta Crystallographica Section B: Structural Crystallography and Crystal Chemistry* **34**, 13220-11323 (1978).
29. Sutter, P., Argyropoulos, C. & Sutter, E. Germanium Sulfide Nano-Optics Probed by STEM-Cathodoluminescence Spectroscopy. *Nano Lett* **18**, 4576-4583 (2018).
30. Kociak, M. & Zagonel, L. F. Cathodoluminescence in the scanning transmission electron microscope. *Ultramicroscopy* **176**, 112-131 (2017).
31. Hentschel, M., Schäferling, M., Duan, X., Giessen, H. & Liu, N. Chiral plasmonics. *Science Advances* **3**, e1602735 (2017).
32. Sutter, E. A. & Sutter, P. W. Size-Dependent Phase Diagram of Nanoscale Alloy Drops Used in Vapor− Liquid− Solid Growth of Semiconductor Nanowires. *Acs Nano* **4**, 4943-4947 (2010).
33. Wei, P.-C., Chattopadhyay, S., Yang, M.-D., Tong, S.-C., Shen, J.-L., Lu, C.-Y., Shih, H.-C., Chen, L.-C. & Chen, K.-H. Room-temperature negative photoconductivity in degenerate InN thin films with a supergap excitation. *Physical Review B* **81**, 045306 (2010).
34. Tan, D., Lim, H. E., Wang, F., Mohamed, N. B., Mouri, S., Zhang, W., Miyauchi, Y., Ohfuchi, M. & Matsuda, K. Anisotropic optical and electronic properties of two-dimensional layered germanium sulfide. *Nano Res.* **10**, 546-555 (2017).

MOVE REFERENCES TO METHODS!!

Supplementary Information is available in the online version of the paper.

Acknowledgements The synthesis of twisted GeS nanowires, analysis of nanobeam diffraction, and transport measurements were supported by the National Science Foundation, Division of Materials Research, Solid State and Materials Chemistry Program under Grant No. DMR-1607795. The development of nanobeam electron diffraction correlated with locally excited cathodoluminescence spectroscopy measurements and analysis was supported by the U.S. Department of Energy, Office of Science, Basic Energy Sciences, under Award No. DE-SC0016343.

Author Contributions P.S. and E.S. planned the study, carried out the nanowire growth and the measurements, and analysed the data. S.W. analysed the electron diffraction data and performed device fabrication and transport measurements. P.S. and E.S. wrote the paper, and all authors commented on the manuscript.

Author Information Reprints and permissions information is available at

www.nature.com/reprints. The authors declare no competing financial interests. Correspondence and requests for materials should be addressed to E.S. (esutter@unl.edu) or P.S. (psutter@unl.edu).

Figures and Figure Legends

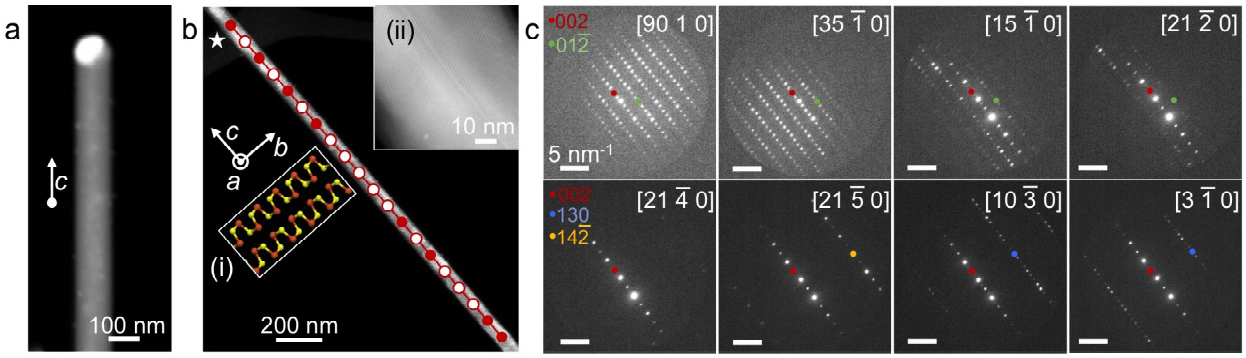

Figure 1. Twisted van der Waals nanowires. a. HAADF-STEM image of a layered germanium sulfide (GeS) nanowire formed by Au-catalyzed vapor-liquid-solid growth. **b.** Section of a GeS nanowire, analyzed by nanobeam diffraction. Insets: (i) Layered GeS structure near the top left segment of the nanowire, ★; (ii) high-resolution STEM, showing layering with 1.06 nm periodicity along the wire axis. **c.** Selected nanobeam electron diffraction patterns at positions along the nanowire marked by red dots in b. Indices [*h k l*] denote the actual zone axis of the nanowire, starting near [1 0 0] and showing progressive twist of the lattice along the nanowire axis.

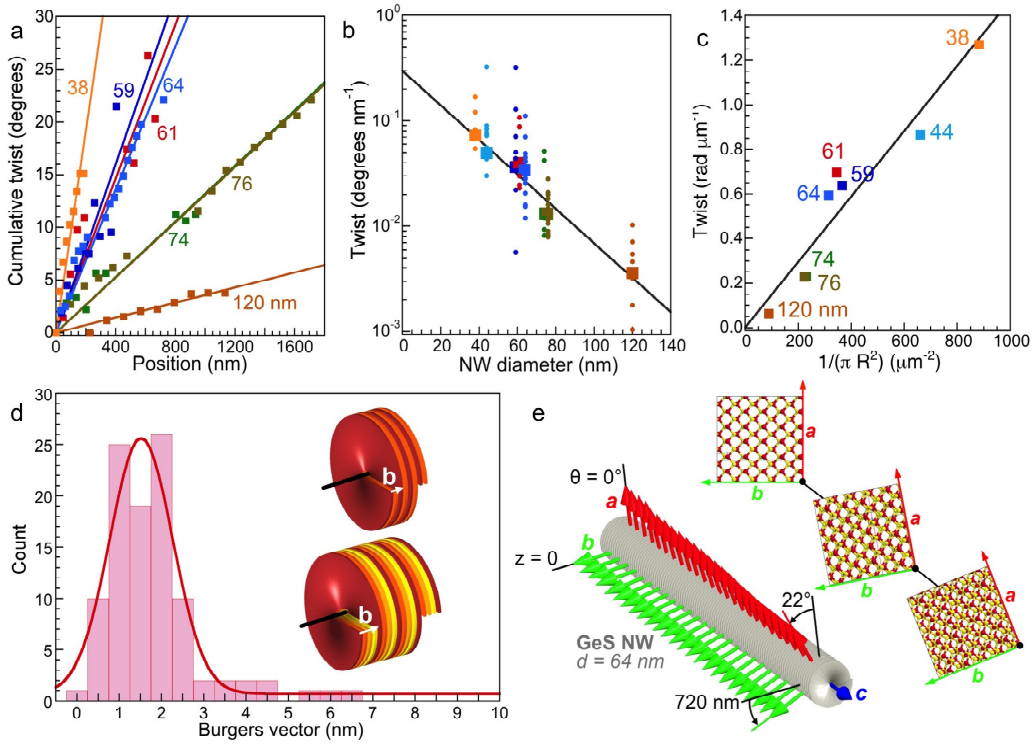

Figure 2. Eshelby twist of layered GeS nanowires. a. Measured cumulative twist angle along selected GeS nanowires and its dependence on wire diameter between 38 – 120 nm. **b.** Scatter plot of the twist per unit length for the nanowires shown in a. Large symbols: Mean twist per nm with exponential dependence on nanowire diameter. **c.** Mean Eshelby twist of the wires shown in a., and linear fit giving a mean Burgers vector **b** = 1.5 nm, i.e., ~3L (GeS layer spacings), of the axial screw dislocation. **d.** Histogram of Burgers vectors for the full data set shown in a., showing preference for values of 2L and 4L Red line: Gaussian fit to the data. Inset: Illustration of twisted van der Waals nanowires with 2L and 4L Burgers vectors. **e.** Schematic showing the rotation of the (*a*, *b*) crystal axes and the change in moiré registry along a chiral GeS nanowires.

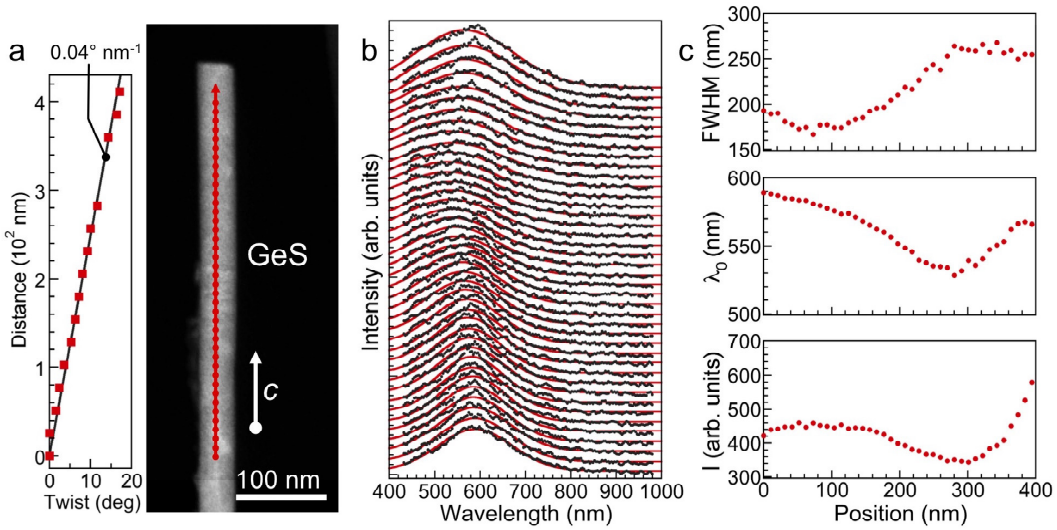

Figure 3. Optoelectronics of twisted GeS nanowires. a. HAADF-STEM image of a section of a GeS van der Waals nanowire and plot of cumulative twist determined by nanobeam diffraction analysis, showing progressive twist $d\theta/dz = 0.04°\ nm^{-1}$. **b.** Series of room-temperature cathodoluminescence spectra obtained at points marked in a. (STEM image, red dots). Red lines: Gaussian fits to the spectra. **c.** Parameters of the Gaussian fits along the GeS nanowire: full width at half maximum (FWHM), center wavelength (λ_0), and peak amplitude (I).

Methods

Synthesis. GeS nanowires were synthesized by vapor-liquid-solid growth via sublimation of GeS powder (99.99%, Sigma Aldrich) in a pumped quartz tube reactor with two temperature zones. In zone #1, a quartz boat with GeS powder (~50 mg) was heated to 450°C. Zone #2 containing the substrate was heated to temperatures between 270-350°C. Si(100) wafers covered with 2-4 nm thick Au films, deposited by sputtering at room temperature and dewetted at the growth temperature, were used as substrates. During growth a carrier gas flow (Ar, 2% H_2) of 50 standard cubic centimeters per minute (sccm) was maintained at a pressure of 20 mTorr. Typical growth times of 10 minutes produced forests of nanowires with lengths of several tens of micrometers. Additional details on growth and characterization can be found elsewhere.[15] The as-grown nanowires contained ubiquitous axial screw dislocations. Among more than 100 GeS nanowires considered, all were found to contain such dislocations. Nanowires for analysis by diffraction and cathodoluminescence were randomly chosen to cover a range of wire diameters and lengths.

Electron Microscopy and Diffraction. The morphology of the nanowires was investigated by (S)TEM in an FEI Talos F200X instrument. Series of nanobeam diffraction patterns were obtained using an incident electron beam with size < 3 nm, displaced in predefined equal steps along the center axis of individual nanowires. Nanobeam diffraction patterns were analyzed using the software package JEMS. First the nearest apparent zone axis (ZA) of each pattern was determined. The simulated sample was then tilted to match the experimental diffraction pattern and determine the actual ZA. To calculate the twist, each ZA [h k l] was considered as [h k 0] and the angle to the [1 0 0] axis determined via the dot product.

Cathodoluminescence Spectroscopy. Cathodoluminescence (CL) spectroscopy was performed in STEM mode (STEM-CL) using a Gatan Vulcan CL holder between T = 110 K – 300 K at 200 kV electron energy. The incident beam current for CL measurements was typically 300-400 pA. Spectrum line scans were acquired by displacing the electron beam in predefined equal steps along individual nanowires and acquiring full CL spectra at each beam position. Typical acquisition times were 10 s per spectrum. Apart from changes in signal to noise ratio, no changes to spectral characteristics were observed for longer or shorter integration times.

Delocalizaton of charge carriers in STEM-CL line scans. To examine the origin of the broad luminescence peaks observed in STEM-CL on twisted GeS nanowires, control experiments were performed on a long (~5 μm) GeS nanowire (Extended Data Fig. 8a). Rather than scanning the exciting electron beam continuously from one end of the wire to the other, five individual STEM-CL spectrum line scans were measured as shown in Extended Data Fig. 8b, i.e., with top-to-bottom scan direction and stitching line scans 1-5 together from bottom to top. This scan pattern was chosen to identify possible displacements of carrier recombination and light emission from the position of the exciting electron beam.

The composite of the five spectrum line scans shown in Extended Data Fig. 8b shows repeated spectral features in consecutive scans, even though the electron beam excitation was seamlessly joined without any overlap. This repetition indicates a spreading of the minority carriers (electrons in the p-type GeS nanowires, see Extended Data Fig. 7). Instead of a symmetric bidirectional spreading expected for delocalization by electron diffusion, Extended Data Fig. 8b shows an asymmetric displacement of the spectral features. This suggests an asymmetric spreading of locally generated carriers, either due to drift in an electric field along the nanowire

axis or spatially varying diffusion coefficient (Extended Data Fig. 9). Both could be caused by the filling of trap states along the nanowire (e.g., at the core of the axial dislocation) by electron-beam excited carriers. An electric field would drive carrier drift along the wire. Via the Einstein relationship, $\frac{D}{\mu} = \frac{kT}{q}$ a transient reduction in carrier mobility (μ) due to scattering by charged traps[33] would translate to a spatially varying diffusion constant (D), causing preferential minority carrier diffusion away from regions excited previously by the electron beam. Additional work is needed to clarify the origin of the directional spreading and recombination of electron-beam excited charge carriers.

Extended Data Fig. 8c shows a lowest-order 'corrected' composite STEM-CL spectrum line scan in which the repeated spectral features have been removed by cutting at dashed lines in Extended Data Fig. 8b, and the overall length re-adjusted to match the dimensions of the nanowire.

Correlation of optoelectronic properties with twist moiré registry. In addition to the data shown in Fig. 3 and Extended Data Fig. 3, series of CL spectra obtained on long GeS nanowires were used to identify signatures of varying electronic structure due to the twist moiré realized in chiral van der Waals nanowires. An example of this type of analysis is shown in Extended Data Fig. 10. Extended Data Fig. 10a shows a diffraction analysis of the cumulative twist along a long GeS nanowire segment. Over a length of 4.6 μm a cumulative twist of 155° is observed. Extended Data Fig. 10b is the composite STEM-CL spectrum line scan along the wire, obtained as shown in Extended Data Fig. 8. The Burgers vector analysis for this wire shows a pronounced peak at 1.1 nm, consistent with a Burgers vector equal to the GeS *c*-axis unit cell size (Extended Data Fig. 10c), i.e., a helical structure with pitch 2L (2 GeS monolayers).

In contrast to planar twisted van der Waals heterostructures, where interlayer twist gives rise to a 2D moiré pattern, chiral layered nanowires project the twist moiré onto a *helical* van der Waals interface. The path across the moiré followed by center of the helix corresponds to the arc in Extended Data Fig. 10d, while the periphery of the helix sweeps along a spiral, as illustrated in Extended Data Fig. 10e. The moiré pattern and arc shown in Extended Data Fig. 10d are drawn to scale for the long chiral GeS nanowire of Extended Data Fig. 10a. Evidently, between points with zone axes (ZA) [010] and [100], i.e., a segment of ~2.6 μm length, the nanowire sweeps through several regions with closely aligned and misaligned GeS lattices at the van der Waals interface (see Extended Data Fig. 10f). The positions of the closely aligned regions of the twist moiré, marked with arrows on the STEM-CL line scan of Extended Data Fig. 10b, show a close correspondence with the luminescence intensity maxima along the nanowire. Other spectral features such as the center wavelength or full width at half maximum (FWHM) are more sensitive to competing effects, including for instance a progressive change in diameter of the slightly tapered nanowire causing an overall red-shift of the spectral center, and local differences in the spreading of excited charge carriers causing differences in peak width. Note that near the end of the nanowire (e.g., Fig. 3), the carrier delocalization is limited so that the electronic effects of a changing moiré registry are visible in the peak center, intensity, and FWHM.

Method References

Data availability. Raw data are included for Figs. 1 and 3a,b and Extended Data Figs. 1; 3; 4 a,b; 5; 6a-e; 7; 8. The full set of diffraction data that support the nanowire twist analysis are available from the corresponding author upon request.

Extended Data Figure Legends

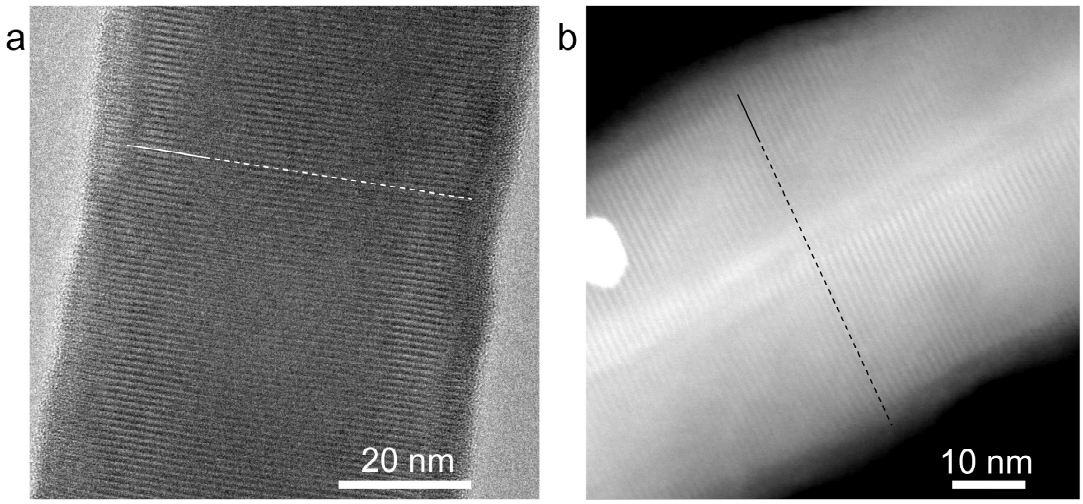

Extended Data Figure 1. Electron microscopy of twisted GeS nanowires with axial screw dislocations. a. High-resolution TEM image of a 65 nm GeS nanowire. The lattice fringes along the wire axis are spaced by 1.06 nm (i.e., the GeS *c*-axis unit cell dimension). **b.** High-resolution STEM image of a 54 nm GeS nanowire. As in a., the lattice fringes along the wire axis are spaced by the GeS *c*-axis unit cell dimension.

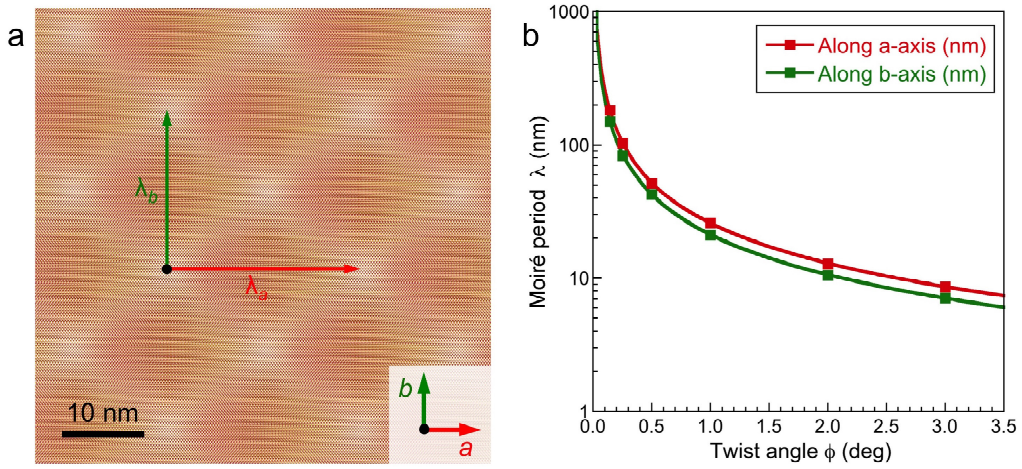

Extended Data Figure 2. GeS twist moiré patterns. a. Illustration of a GeS twist moiré (here with 1° twist angle). Note the reversal of the ratio $\lambda_a/\lambda_b = b/a$, where ($a$, b) denote the in-plane lattice parameters of GeS, and λ_a, λ_b are the moiré periods along the a- and b-directions. **b.** Moiré periodicity for a twisted GeS van der Waals interface as a function of interlayer twist angle. Data points were obtained from overlays of models of two GeS monolayers with different relative orientation. The solid line is a power law fit $\lambda \sim \phi^{-1}$ to the data.

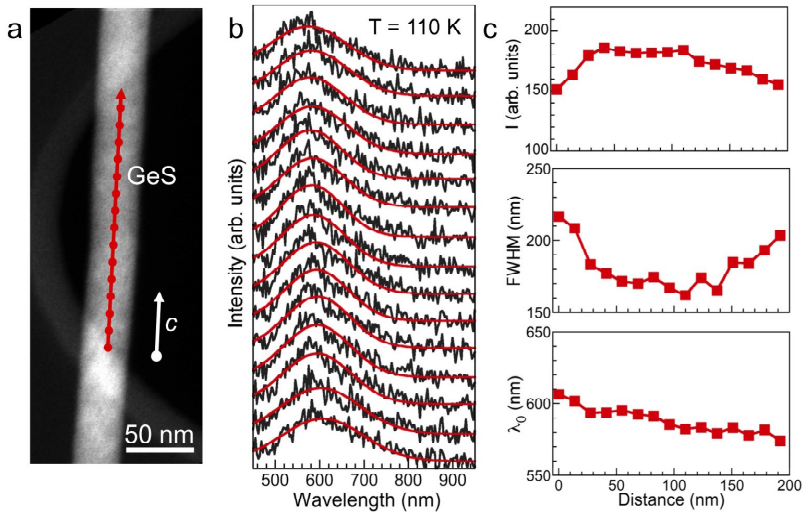

Extended Data Figure 3. STEM-CL line scan along a twisted GeS nanowire measured at T = 110 K. a. HAADF-STEM image of a GeS nanowire (diameter ~44 nm). **b.** Position dependent STEM-CL spectra recorded along the nanowire at points marked in a. (T = 110 K). Lines are Gaussian fits to the dominant band edge luminescence peak. **c.** Plots of the Gaussian fit parameters (amplitude I; full width at half maximum, FWHM; center wavelength, λ_0) as a function of position along the nanowire.

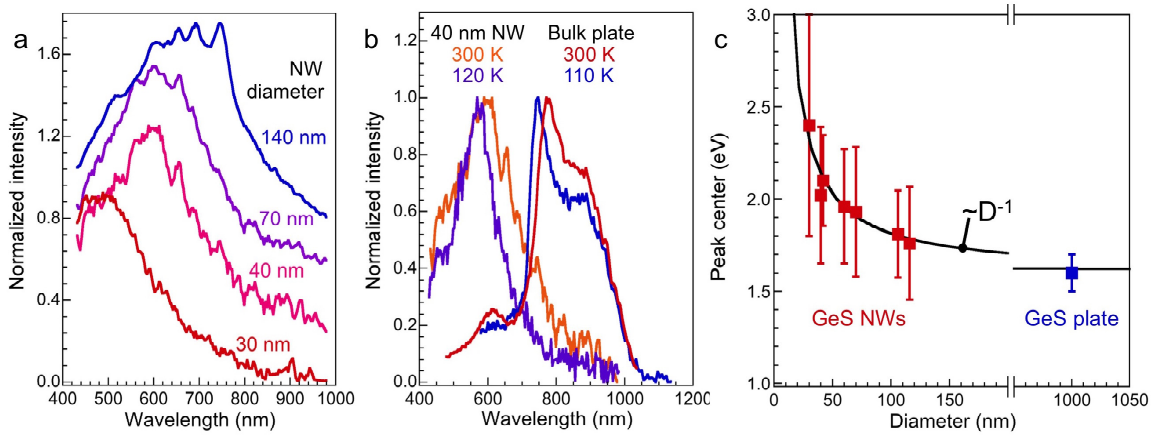

Extended Data Figure 4. Size-dependent GeS band edge luminescence. a. Examples of STEM-CL spectra for GeS nanowires with four different diameters (140 nm, 70 nm, 40 nm, 30 nm) measured at room temperature. Note the progressive blue shift with decreasing nanowire diameter and the intensity modulation for the 140 nm wire, which is due to photonic waveguide mode interference in thick nanowires similar to that observed in planar GeS plates and prisms (see Extended Data Fig. 5).[29] **b.** Comparison of the temperature-dependent CL spectra of a 40 nm diameter GeS nanowire and of a µm-sized, single-crystalline bulk GeS plate; CL spectra were measured at room temperature and at T = 120 K and 110 K, respectively. For nanowires and plates, the luminescence peak narrows and blue shifts by the same amount (~30 nm) at low temperature. **c.** Analysis of the peak photon energy of the CL spectra of GeS nanowires with different diameters, D, and of a bulk GeS plate (lateral size ~1 µm). Error bars are based on the full width at half maximum (FWHM) of the luminescence peaks. The black line is a fit $h\nu \sim D^{-1}$, with a bulk bandgap of 1.60 eV.[29]

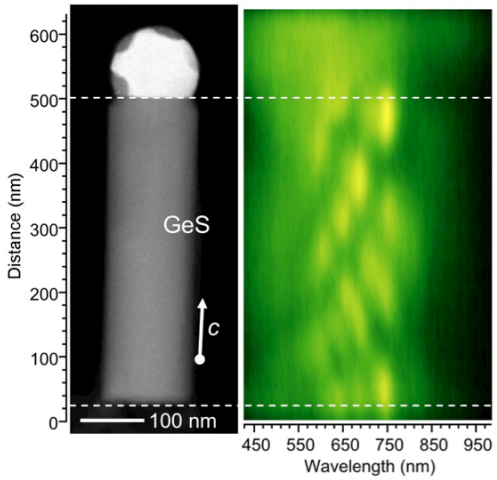

Extended Data Figure 5. Waveguide mode interference in thick GeS nanowires. HAADF-STEM image of a 140 nm thick nanowire near the Au-rich VLS catalyst (left), and STEM-CL line scan along the center axis of the wire (right) showing fringes due to interference of traveling waveguide modes reflected by the specular end facets of the nanowire.[29]

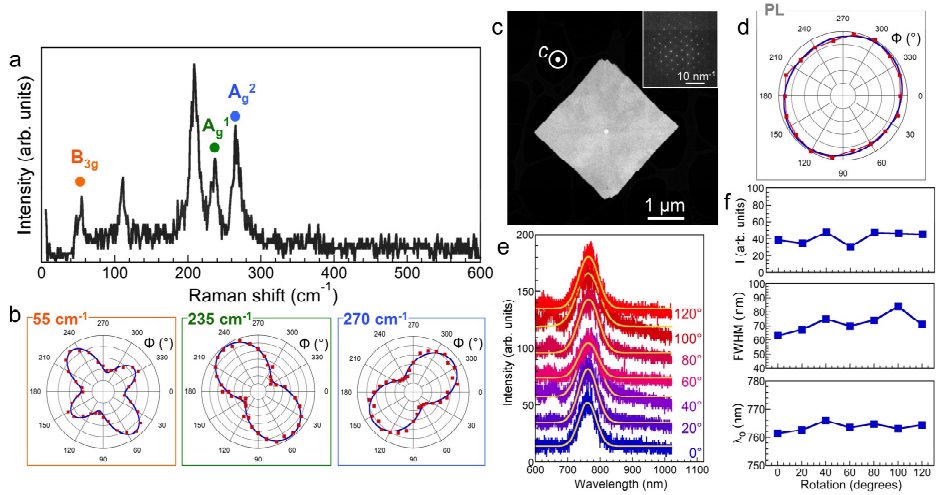

Extended Data Figure 6. Polarized Raman and photoluminescence on mesoscale monocrystalline GeS plates. a. Raman spectrum on a monocrystalline GeS plate with linearly polarized laser light (λ = 532 nm) incident along the *c*-axis, showing the B_{3g} and A_g modes associated with the orthorhombic layered crystal. **b.** Polar plots of Raman intensity as a function of the polarization direction of the incident light for three different modes. Note the strongly anisotropic Raman scattering by the single-crystalline GeS plate.[34] **c.** HAADF-STEM image of a mesoscale GeS plate. The *c*-axis lies perpendicular to the large top facet of the plate. Inset: Electron diffraction pattern of the GeS plate. **d.** Polar plot of band edge photoluminescence (PL) intensity as a function of the polarization of the exciting laser beam (λ = 532 nm). **e.** PL spectra for different orientation of the GeS plate relative to the polarization of the incident light. Lines show Gaussian fits to the main peak. **f.** Plots of the parameters of the Gaussian fits for different rotation angles of the plate relative to the incident light polarization: Amplitude (I), full width at half maximum (FWHM), center wavelength (λ_0). Polarization dependences were measured on individual GeS plates using a Horiba Scientific XPlora Plus Raman/PL microscope with angle between sample and incident light polarization varied using a sample rotation stage.

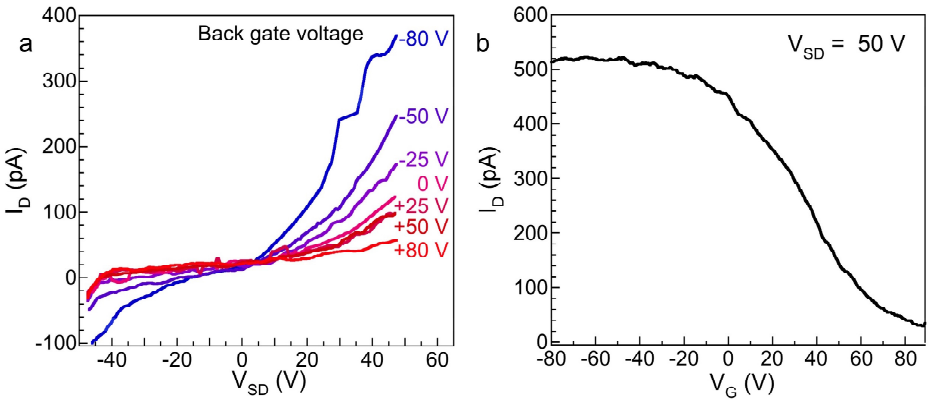

Extended Data Figure 7. Gated charge transport in twisted GeS nanowires. a. Drain-current as a function of source-drain bias measured at room temperature for a single GeS nanowire field-effect transistor (FET) back gated via 300 nm SiO_2/Si. Nanowire diameter: 116 nm. Channel length: 5 μm. **b.** Transfer characteristics (drain current as a function of back gate voltage) for the GeS nanowire FET. For transport measurements, Ti/Au contacts (10/60 nm) were deposited on single GeS nanowires using patterning with electron beam lithography; transport measurements were made on a Lakeshore probe station under vacuum ($1x10^{-7}$ Torr) at room temperature.

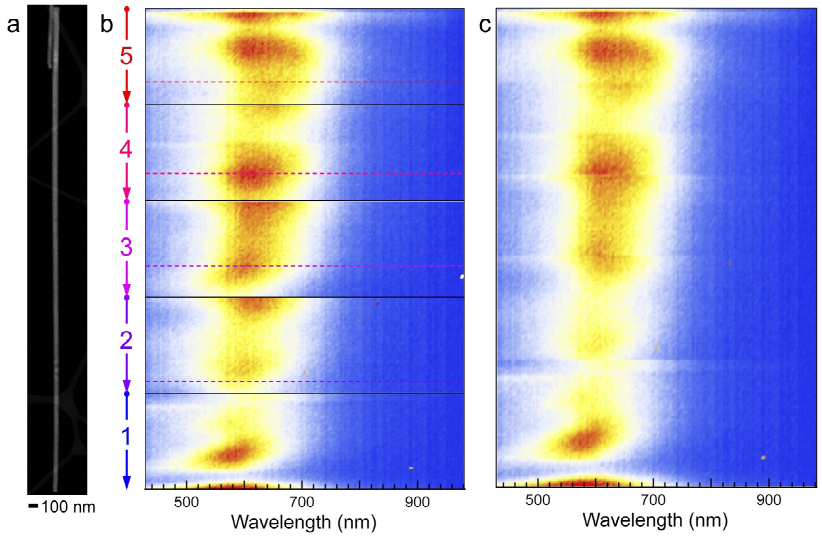

Extended Data Figure 8. STEM-CL line scans on a long GeS nanowire (T = 300 K). a. HAADF-STEM image of the ~5 μm GeS nanowire. **b.** STEM-CL spectrum line scan, obtained in five consecutive sections scanned as shown by arrows. The particular scan pattern was chosen to identify displacements of charge carrier recombination from the position of the exciting electron beam. Note the repetition of spectral features, even though the electron-beam excitation was precisely stitched in consecutive line scans. **c.** Reconstruction of the CL spectra along the nanowire by cutting repeated sections along dashed lines shown in b.

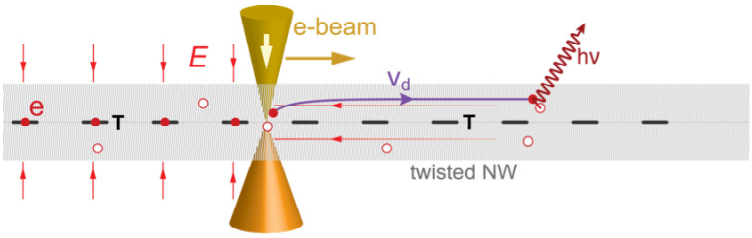

Extended Data Figure 9. Schematic of asymmetric minority carrier drift or diffusion along the GeS nanowires. Illustration of the two possible mechanisms discussed above, both related to the filling of charge traps (T) by electron-beam excited carriers: (i) Drift (v_d) due to a net electric field along the wire axis; or (ii) charged impurity scattering causing differences in carrier mobility and diffusion coefficient. In line scans as shown in Extended Data Fig. 8, both mechanisms would cause light emission predominantly downstream (i.e., in areas not yet scanned by the electron beam) from the excitation spot.

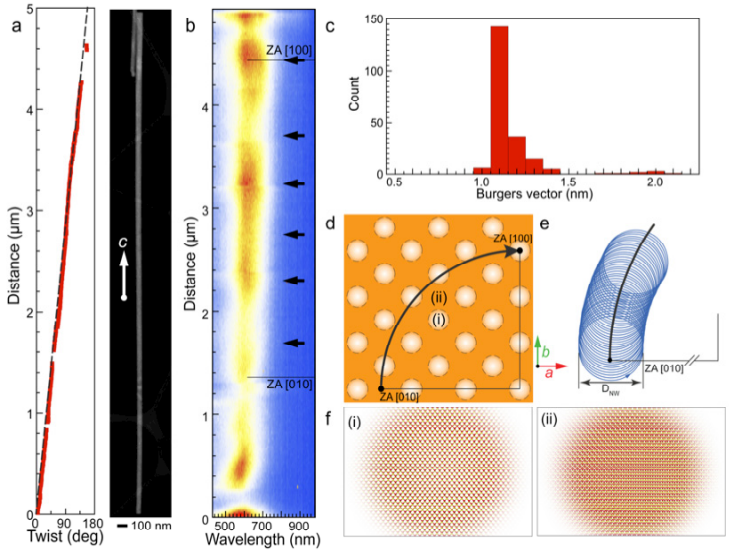

Extended Data Figure 10. Twist and STEM-CL analysis of a long (~5 µm) GeS nanowire section (T = 300 K). a. HAADF-STEM image of the GeS nanowire, and analysis of the cumulative twist angle along the wire. **b.** STEM-CL spectrum line scan of the twisted GeS nanowire, reconstructed from five individual line scans as shown in Supporting Figure S8. The twist angle increases by 90° between points with zone axis (ZA) [010] and ZA [100]. **c.** Histogram of Burgers vectors along the GeS nanowire shown in a., using the same analysis as in Fig. 2 of the paper. **d.** Evolution of the twist moiré registry along the nanowire. White and orange shaded regions indicate sections of a planar twist moiré pattern in which the adjacent GeS layers are closely aligned (white, (i)) or misaligned (orange, (ii)). The arc indicates the progression of the moiré registry between ZA [010] and ZA [100] along the nanowire; it sweeps through several regions with aligned and misaligned GeS layers. The positions of closely aligned regions, marked by arrows in b., coincides approximately with intensity maxima of the STEM-CL spectrum line scan. **e.** Illustration of parts of the spiral path of the periphery of the helical van der Waals interface across the twist moiré pattern (D_{NW}: Nanowire diameter). **f.** Illustration of the closely aligned (i) and misaligned (ii) regions of the twist moiré (drawn here for 0.25° interlayer twist).